Petroleum Science 23 (2026) 4704–4716

Contents lists available at ScienceDirect

Petroleum Science

journal homepage: www.keaipublishing.com/en/journals/petroleum-science

Original Paper

Imaging enhancement for towed-streamer data using OBN data based on deep learning

Zhi-Na Li [a,b,*], He-Xiang Zhang [a,b], Zhen-Chun Li [a,b], Zi-Lin He [a,b], Qi Zhang [a,b], Bo-Xiong Zhao [a,b], Zhi-Chuan Yu [a,b], Qiang Xu [c], Ming-Qiang Zhang [c]

[a] State Key Laboratory of Deep Oil and Gas, China University of Petroleum (East China), Qingdao, 266580, Shandong, China
[b] School of Geosciences, China University of Petroleum (East China), Qingdao, 266580, Shandong, China
[c] China Oilfield Services Limited, Tianjin, 300459, China

ARTICLE INFO

Article history:
Received 6 June 2025
Received in revised form
23 February 2026
Accepted 26 April 2026
Available online 30 April 2026

Edited by Meng-Jiao Zhou

Keywords:
Imaging enhancement
Towed-streamer data
OBN data
Deep learning

ABSTRACT

Deep oil and gas exploration has become a critical frontier in offshore oil and gas development due to growing global energy demand. However, traditional towed-streamer seismic acquisition often struggles to deliver high-resolution imaging of deep and structurally complex subsurface targets. A promising solution is to integrate towed-streamer data with ocean bottom node (OBN) data, which provide broader azimuthal coverage, full-offset sampling, and multi-component recording, thereby complementing streamer acquisition and enhancing image quality. Despite these advantages, conventional fusion methods—typically based on simple linear weighted averaging—are often inadequate for effectively combining the distinct characteristics of OBN and streamer images. Such approaches risk producing inappropriate subsurface representations. To address this limitation, this paper proposes a novel deep learning-based imaging enhancement strategy for the joint utilization of OBN and streamer seismic data in this paper. By leveraging the nonlinear representation capabilities of neural networks, the proposed method learns to adaptively extract and fuse complementary features from both datasets, yielding more coherent, high-resolution, and geologically consistent imaging results. This study begins with a comparative analysis of the imaging characteristics of streamer and OBN data, followed by the design of a tailored deep learning architecture for data fusion. Numerical experiments confirm the feasibility and robustness of the approach. The results demonstrate improved reflector continuity, amplitude fidelity, and structural clarity compared to conventional methods, especially in the complex cases, highlighting the method's potential for advancing subsurface imaging in deep oil and gas exploration scenarios.

1. Introduction

Deep oil and gas exploration has become a critical focus in offshore oil and gas exploration. Conventional towed-streamer seismic exploration is constrained by cable length, which restricts the offset range and hinders detailed imaging of deep-layer and complex structures (Walker et al., 2023). Ocean bottom node (OBN) data, with large offsets and multi-component acquisition, has emerged as a promising solution to provide enhanced illumination in complex subsurface environments. However, OBN acquisition is costly and time-consuming, and the sparse distribution of geophones can significantly reduce the signal-to-noise ratio of shallow migration profiles (Alerini et al., 2009).

Due to its inherent limitations, OBN cannot completely replace towed-streamer exploration, but it can effectively complement the deep imaging of towed-streamer data. Considering the advantages of OBN, a series of attempts have been made to supplement towed-streamer imaging with OBN data. Wong et al. (2012) and Poole (2021) developed jointly constrained inversion-based imaging methods for integrating towed-streamer and OBN data using synthetic and field datasets, respectively, demonstrating that this strategy can effectively combine the broad illumination of OBN data with the superior lateral resolution provided by towed-streamer

* Corresponding author.
E-mail address: lizhina00@163.com (Z.-N. Li).
Peer review under the responsibility of China University of Petroleum (Beijing).

https://doi.org/10.1016/j.petsci.2026.04.040

data. Yu et al. (2021, 2023) introduced a joint elastic reverse time migration (ERTM) method for towed-streamer and sparse OBN data. Yang and Zhang (2022) optimized imaging by inputting towed-streamer and OBN data with depth-weighted inputs through imaging domain least squares reverse time migration (ID-LSRTM). Besides these data-domain methods, another feasible strategy is the combination of migration results. Granger et al. (2005) merged the imaging results of towed-streamer and OBN using a matching operator, while Li et al. (2022) combined the RTM results of both through a coherence-based weighting strategy. However, these methods result in a uniform linear weighting (in depth or frequency) across the entire imaging region, which may fail to achieve targeted enhancement in areas with weak illumination. Furthermore, they may disrupt the relative energy and waveform relationships of the images, and waveform matching, in turn, introduces additional computational costs.

In recent years, deep learning has demonstrated substantial potential in seismic data processing, achieving notable results in FWI (Singh et al., 2021; Alfarhan et al., 2023) and migration (Liu et al., 2020; Torres and Sacchi, 2021; Sun et al., 2023a). More importantly, it has already shown its advantages in related image processing tasks such as noise suppression (Sun et al., 2023b), low-frequency information reconstruction (Aharchaou and Baumstein, 2020), and resolution enhancement (Halpert, 2018). These advancements provide new solutions for efficiently and stably addressing imaging enhancement. For example, Malikov et al. (2024) employed two independent U-Net architectures to achieve denoising and vertical resolution enhancement of post-stack seismic data, respectively, effectively improving image quality. Cheng et al. (2023) utilized a multi-scale convolutional neural network (Ms-CNN) to map the migration results of sparse OBN data to dense data images, thereby compensating for the insufficient shallow illumination of OBN and restoring the shallow structural morphology. A well-trained deep neural network can address issues such as weak reflection energy, discontinuous events, and other problems caused by insufficient illumination in the migration results, while also suppressing noise within.

To overcome the shortcomings of traditional methods and obtain high-quality images, this paper proposes a deep-learning-based imaging enhancement strategy. We treat this process as an image processing problem, training a deep convolutional neural network model based on deep parts of migration profiles from OBN and towed-streamer data. The trained network model is then utilized to process the migration results of streamer data, thereby enhancing its deep illumination and resolution. The structure of this paper is organized as follows. First, we review the imaging principles of towed-streamer and OBN data, highlighting their respective advantages and limitations. Next, we introduce the deep neural network architecture used for training and propose a specialized data generation strategy tailored to enhance towed-streamer imaging. To establish a robust mapping relationship between towed-streamer and OBN imaging results, we then formulate the network training and prediction processes in detail. Finally, the proposed method is validated through a series of experiments on both synthetic and field datasets, demonstrating its feasibility and effectiveness in imaging enhancement of the towed-streamer data.

2. Methodology

2.1. Imaging of towed-streamer and OBN data

To better understand the complementary advantages of different acquisition systems in seismic imaging, it is essential to analyse the characteristics of both towed-streamer and OBN data. Fig. 1 briefly illustrates the acquisition geometries of towed-streamer and OBN systems. In towed-streamer acquisition, receivers are positioned on only one side of the source, resulting in limited offsets that restrict the illumination of deep targets, especially those with steep dips. In contrast, OBN systems can capture wavefields from all directions with much larger offsets, providing broader illumination and improving deep imaging. However, due to the high cost of OBN deployment, the node spacing is typically sparse—often several hundred meters—which significantly degrades the signal-to-noise ratio in shallow imaging. Each acquisition system presents distinct advantages and limitations. Towed-streamer acquisition remains the most widely used marine seismic method owing to its cost efficiency, technological maturity, and the extensive availability of legacy data. By complementing the shallow-to-intermediate imaging strengths of towed-streamer data with the superior deep imaging capability of OBN systems, their joint utilization holds strong potential for improving the imaging quality of complex deep structures.

Reverse-time migration (RTM) is particularly well-suited for subsalt, steep-dip, and complex geological environments. Considering its imaging advantages, we adopt RTM to image both towed-streamer and OBN seismic data. For towed-streamer data, conventional RTM is typically performed using the cross-correlation imaging condition, which can be expressed as:

$$I^P_{\mathrm{ts}}(x,z) = \sum_{t=0}^{t_{\max}} S(x,z,t) \cdot P_{\mathrm{ts}}(x,z,t), \tag{1}$$

where S and P denote the forward-propagated source wavefield and the backward-propagated receiver (primary) wavefield, respectively. The subscript ts denotes towed-streamer data. $t_{\max}$ is the recording time. I^P_{ts} is the image for the towed-streamer dataset. To improve the accuracy of migration, preprocessing steps such as deghosting and surface-related multiple suppression must be applied. However, the finite acquisition aperture and restricted offset range of towed-streamer systems fundamentally limit their illumination of deeper subsurface structures and steeply dipping interfaces, a challenge that becomes more pronounced in deep-layer settings.

In contrast, OBN data provide a more favorable acquisition geometry for complex imaging scenarios. Due to the seabed deployment of sensors, OBN can record both up-going and down-going wavefields, offering full azimuth coverage and long-offset data. The OBN data can be decomposed into the up-going wavefield and the down-going wavefield. Since primaries are typically characterized by up-going wavefields, whereas multiples comprise both up-going and down-going components, the wavefield can thus be decomposed as follows:

$$R_{\mathrm{obn}}(x,z,t) = P_{\mathrm{obn}}(x,z,t) + M^{\mathrm{u}}_{\mathrm{obn}}(x,z,t) + M^{\mathrm{d}}_{\mathrm{obn}}(x,z,t), \tag{2}$$

where R is the recorded seismic data, M represents the multiples, and the subscripts u and d represent up-going and down-going waves, superscript obn denotes OBN data.

However, current OBN imaging predominantly relies on conventional up-going primary imaging. Accordingly, the RTM-based imaging process can be formulated as follows:

$$I^P_{\mathrm{obn}}(x,z) = \sum_{t=0}^{t_{\max}} S(x,z,t) \cdot P_{\mathrm{obn}}(x,z,t), \tag{3}$$

where I^P_{obn} is the OBN imaging result. While OBN data offer superior deep imaging capabilities, their sparse spatial sampling—often with node spacing up to several hundred meters due to high acquisition cost and operational complexity—leads to degraded resolution and

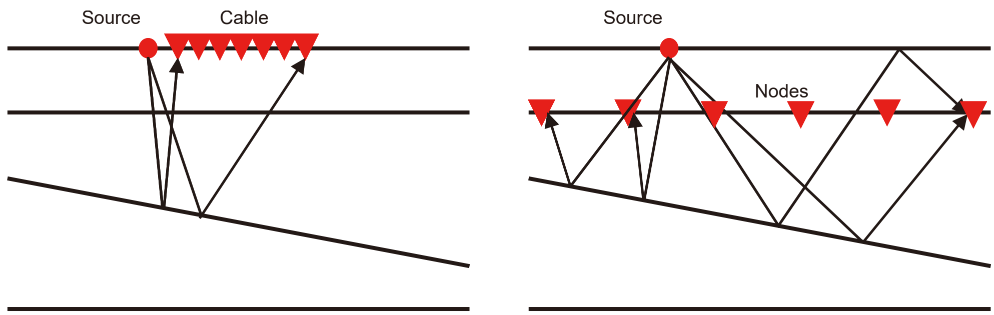

Fig. 1. Illustration of towed-streamer and OBN acquisition geometries.

severe acquisition footprints in the shallow section when conventional primary-only imaging is applied.

Multiple imaging is recognized as an effective technique for enhancing subsurface illumination. To address these challenges, we apply the mirror migration method to OBN data. As shown in Fig. 2, mirror migration utilizes the down-going first-order multiples for imaging. Its principle involves virtually mirroring the seabed receivers above the sea surface; the required down-going wavefield is then treated as equivalent up-going waves for imaging (Pacal et al., 2015). As illustrated in Fig. 2, the green and blue circles denote the illumination regions contributed by the seabed receivers and their mirrored counterparts, respectively. This virtual source-receiver geometry effectively increases the illumination aperture and enhances the coverage of shallow and intermediate depth structures.

Accurate separation of up-going and down-going wavefields in OBN data is critical for ensuring the imaging accuracy of mirror migration methods that rely on the down-going wavefield. In OBN acquisition, both pressure (p) and vertical velocity component (v_z) are recorded at each seabed node. For up-going waves, these two components share the same polarity; however, for down-going waves, they exhibit opposite polarities. This polarity difference provides a physical basis for wavefield separation. By applying amplitude, phase, and frequency matching between the pressure and vertical velocity records, one can isolate the down-going component through subtraction (Barr, 1997), which is widely used in practice. However, this method is incapable of distinguishing between down-going multiples of different orders. If the separated down-going wave data are directly utilized for imaging, artifacts will emerge in the imaging process described by Eq. (4).

$$I_{\mathrm{obn}}^{\mathrm{m}}(x,z)=\sum_{t=0}^{t_{\max}}S(x,z,t)M_{\mathrm{obn}}^{\mathrm{d}}(x,z,t), \tag{4}$$

with $$M_{\mathrm{obn}}^{\mathrm{d}}(x,z,t)=M_{\mathrm{obn}}^{\mathrm{d}_1}(x,z,t)+M_{\mathrm{obn}}^{\mathrm{d}_2}(x,z,t)+\cdots, \tag{5}$$

where $I_{\mathrm{obn}}^{\mathrm{m}}$ is the imaging result using down-going waves, and $M_{\mathrm{obn}}^{\mathrm{d}}$ is the down-going multiples in the OBN data. Since all down-going waves are composed of multiples, the down-going wavefield $M_{\mathrm{obn}}^{\mathrm{d}}$ can be further expressed as a summation of multiple reflections of different orders. Specifically, $M_{\mathrm{obn}}^{\mathrm{d}_1}$ and $M_{\mathrm{obn}}^{\mathrm{d}_2}$ denote the first-order and second-order down-going multiples, respectively. Further, Eq. (4) can be re-expressed as

$$I_{\mathrm{obn}}^{\mathrm{m}}(x,z)=\sum_{t=0}^{t_{\max}}S(x,z,t)M_{\mathrm{obn}}^{\mathrm{d}_1}(x,z,t)+\sum_{t=0}^{t_{\max}}S(x,z,t)M_{\mathrm{obn}}^{\mathrm{d}_2}(x,z,t)+\cdots. \tag{6}$$

On the right-hand side of the equation, the first term contributes constructively to the true image in the mirror migration process, whereas the second and the other terms introduces image artifacts. As illustrated in Fig. 3, the artifact—highlighted by the red circle—is caused by the inclusion of second-order multiples, ultimately degrading the accuracy and quality of the final migrated image when all down-going multiples are used indiscriminately.

Unlike conventional marine seismic acquisition systems (e.g., towed-streamer), the seismic source and geophones in OBN systems are positioned at different interfaces, leading to a significant datum difference. As a result, the datum inconsistency prevents the direct application of conventional surface-related multiple elimination (SRME)-based methods (Li et al., 2017) for multiple separation. Some studies have demonstrated that by incorporating towed-streamer data, the SRME method can be extended to OBN data, yielding favorable application outcomes (Ikelle, 1999; Zhong et al., 2014). Within this extended SRME context, the high-order down-going wavefield components present in OBN data can be

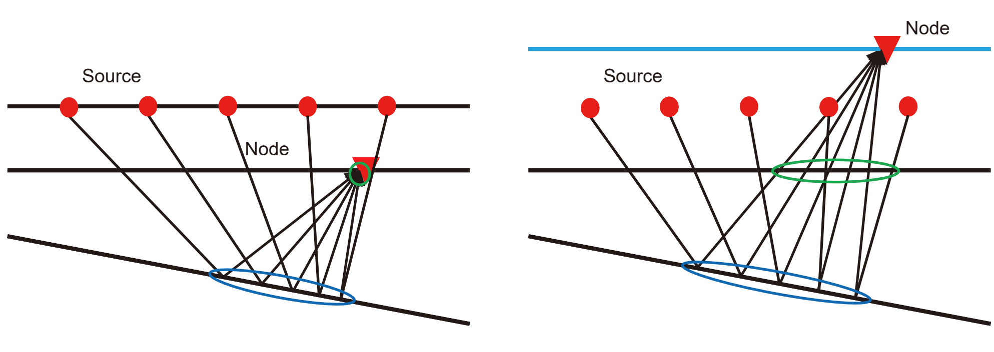

Fig. 2. Illumination of up-going and down-going wave imaging.

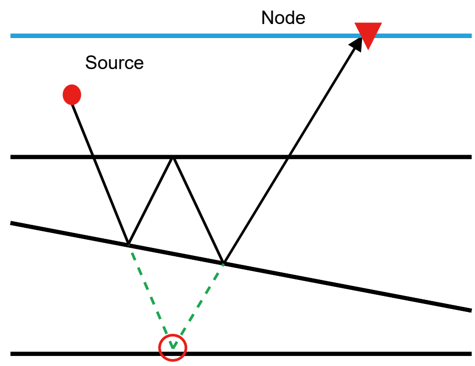

Fig. 3. Illustration of multiple-wave imaging artifact.

expressed as a convolution between the OBN down-going wavefield and the towed-streamer wavefield. Through this approach, the first-order down-going multiples $M_{\mathrm{obn}}^{\mathrm{d_1}}$ required for mirror migration can be separated from the entire down-going wavefield $M_{\mathrm{obn}}^{\mathrm{d}}$:

$$\widehat{M}_{\mathrm{obn}}^{\mathrm{d}}(x_{\mathrm{s}}, x_{\mathrm{r}}, t) = M_{\mathrm{obn}}^{\mathrm{d}}(x_{\mathrm{s}}, x_{\mathrm{r}}, t) \otimes R_{\mathrm{ts}}(x_{\mathrm{s}}, x_{\mathrm{r}}, t), \tag{7}$$

$$M_{\mathrm{obn}}^{\mathrm{d_1}}(x_{\mathrm{s}}, x_{\mathrm{r}}, t) = M_{\mathrm{obn}}^{\mathrm{d}}(x_{\mathrm{s}}, x_{\mathrm{r}}, t) - b(x_{\mathrm{s}}, x_{\mathrm{r}}, t) \otimes \widehat{M}_{\mathrm{obn}}^{\mathrm{d}}(x_{\mathrm{s}}, x_{\mathrm{r}}, t). \tag{8}$$

Here, $\widehat{M}_{\mathrm{obn}}^{\mathrm{d}}$ is the predicted multiples, $M_{\mathrm{obn}}^{\mathrm{d}}$ and R_{ts} denote the OBN down-going wavefield and the towed-streamer wavefield, respectively. x_{s} and x_{r} represent the locations of the sources and receivers, while $M_{\mathrm{obn}}^{\mathrm{d_1}}$, $M_{\mathrm{obn}}^{\mathrm{d_2}}$, etc., symbolize down-going multiples of different orders, and b stands for the matching operator. The matching operator b is first obtained through inversion by solving the following least-squares problem:

$$J(b) = \left\| M_{\mathrm{obn}}^{\mathrm{d}} - b \otimes \widehat{M}_{\mathrm{obn}}^{\mathrm{d}} \right\|_2^2, \tag{9}$$

Once the operator b is solved, it can be substituted into Eq. (8) to get the separated first-order down-going multiples. The finally separated first-order down-going multiple $M_{\mathrm{obn}}^{\mathrm{d_1}}$ can serve as the input for mirror migration. The imaging process can be described by Eq. (10) as follows:

$$I_{\mathrm{obn}}^{\mathrm{m_1}}(x, z) = \sum_{t=0}^{t_{\max}} S(x, z, t) \cdot M_{\mathrm{obn}}^{\mathrm{d_1}}(x, z, t). \tag{10}$$

Here, $I_{\mathrm{obn}}^{\mathrm{m_1}}$ represents the result of mirror migration. The mirror migration using first-order multiples can increase the receiving aperture, thereby improving imaging quality. However, when the nodes are relatively sparse, acquisition footprints cannot be completely eliminated, leading to certain limitations in the imaging accuracy of shallow layers.

2.2. Network architecture

To improve the imaging quality of towed-streamer data in deep layers and structurally complex environments, while avoiding acquisition footprints in shallow layers caused by sparse OBN data acquisition, this study explores the use of OBN data to improve towed-streamer imaging results. Conventional fusion approaches typically apply a uniform linear-weighted stacking to the entire image, which fails to provide localized enhancement in poorly illuminated target zones. Considering the advantages of deep learning in data fusion and feature extraction, we propose a deep learning-based method for imaging enhancement by integrating two different types of imaging data. This method develops a network architecture that characterizes the mapping relationship between the limited-illumination imaging results of towed-streamer data and the broader-illumination imaging results of OBN data.

This paper aims to achieve imaging optimization by defining a U-Net architecture within the TensorFlow framework. Derived from fully convolutional neural networks, the U-Net network boasts powerful feature extraction and fusion capabilities, along with a clear, modifiable structure. U-Net and its extended architectures have been widely applied in various image processing tasks and are increasingly being adopted in the field of seismic exploration. A series of studies have utilized U-Net for applications such as illumination compensation (Shi et al., 2024), image processing (Wu et al., 2024), and data matching (Zhang et al., 2021), demonstrating its performance advantages. Our primary objective is to compensate illumination by training on the seismic images, which can be regarded as a matching process; therefore, U-Net is adopted as the network architecture. Its encoder-decoder structure with skip connections effectively captures multi-scale features while preserving detailed information, which is crucial for seismic image fusion. We anticipate leveraging the nonlinear capabilities of deep neural networks to quickly obtain high-quality migration results.

The U-Net architecture employed in this study is shown in Fig. 4(a), consisting of an encoder module (left panel) and a decoder module (right panel). The encoder's function is to learn the features of the input image by performing four down-samplings using max pooling. Correspondingly, the data compressed by the encoder will be reconstructed in the decoder, with bilinear interpolation selected as the up-sampling method. The left and right sides of the network are connected by convolutional layers. Additionally, skip connections link the encoding layers and decoding layers at the same level to achieve data feature fusion. The fundamental U-net network comprises 27 hidden layers, with a selected convolution kernel size of 3×3 and a sliding stride of 1. The number of convolution kernels in each layer is 32, 64, 64, 128, 128, 128, 256, 256, 256, 512, 512, 512, 1024, 1024, 1024, 512, 512, 512, 256, 256, 256, 128, 128, 128, 64, 64 and 32, respectively. The output is produced through a final convolutional layer with a kernel size and number of 1. Batch normalization layers and activation functions are applied after each convolutional layer. Building upon this baseline architecture, we replace two adjacent convolutional layers with a residual block, as illustrated in Fig. 4(b). By introducing a shortcut connection that carries an identity mapping, the network's feature extraction capability is further enhanced. This residual learning strategy mitigates the vanishing gradient problem in deeper networks and improves the overall stability and performance of the model.

Except for the last layer, the LeakyReLU function is used as the activation function to enhance the nonlinear characteristics of the data and the stability of network training.

$$\mathrm{LeakyReLU}(\varepsilon) = \begin{cases} \varepsilon, & m \geq 0 \\ \alpha\varepsilon, & m < 0 \end{cases}, \tag{11}$$

where ε denotes the input data, the parameter α is set to 0.02. For the last convolutional layer, since the data has been normalized

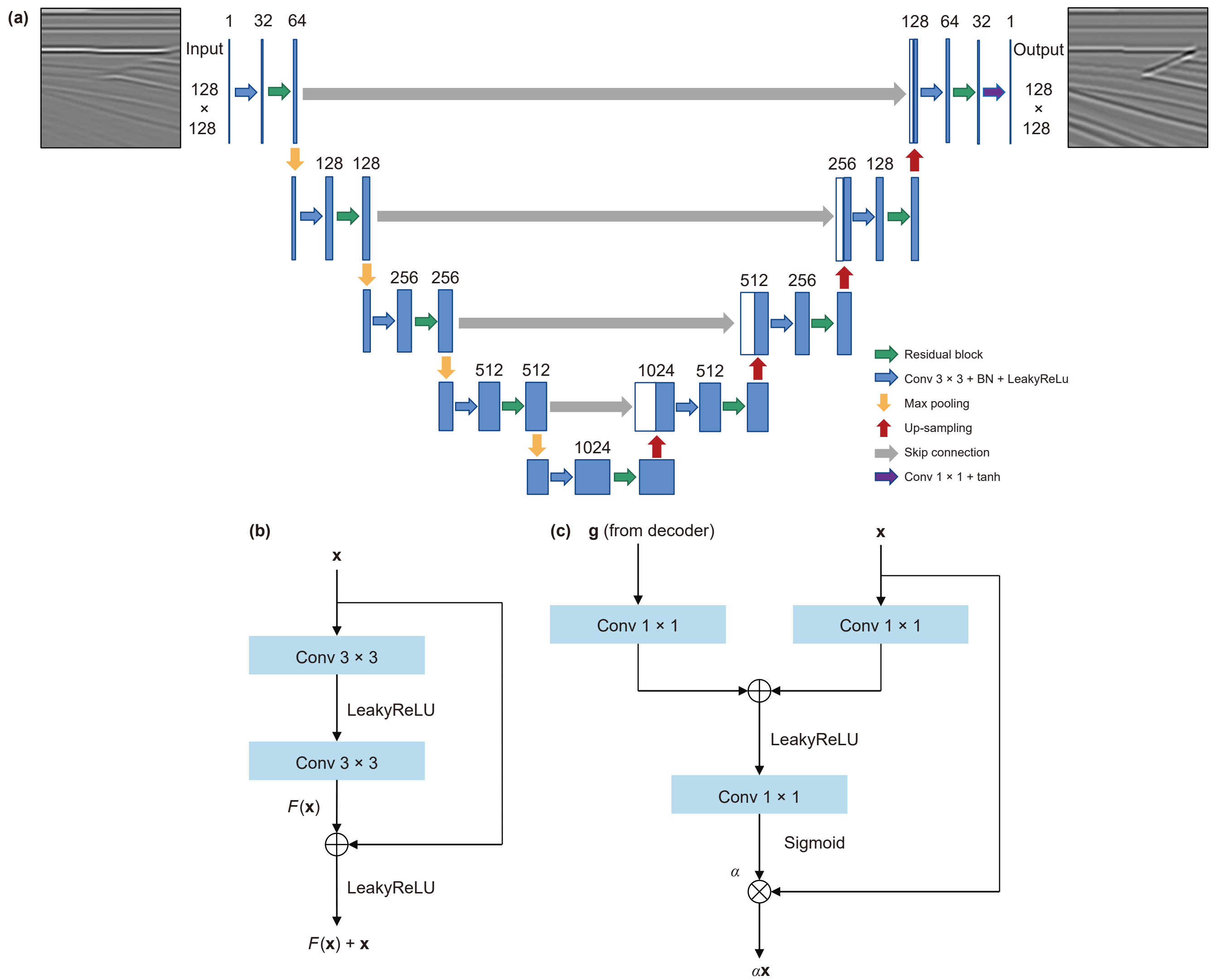

Fig. 4. Visualization of network architecture. **(a)** U-Net, **(b)** residual block, **(c)** attention gate.

beforehand with values within the range of $[-1, 1]$, the hyperbolic tangent function (tanh) is chosen as the activation function

$$\tanh(\varepsilon) = \frac{\sinh(\varepsilon)}{\cosh(\varepsilon)} = \frac{e^{\varepsilon} - e^{-\varepsilon}}{e^{\varepsilon} + e^{-\varepsilon}}. \tag{12}$$

In conventional U-Net architectures, skip connections directly concatenate low-level semantic features from the encoder into the decoder. However, there often exists a noticeable semantic gap between the encoder feature maps and the decoder feature representations. Furthermore, seismic migration sections tend to contain a considerable amount of redundant or irrelevant information, with key geological features—such as faults and salt boundaries—sometimes occupying only a small proportion. This results in encoder outputs that often include substantial background noise unrelated to target zones. Therefore, direct feature concatenation is not always optimal for effective feature fusion, especially for our image fusion. To address this limitation and better adapt the U-Net architecture to image enhancement, we introduce attention gates (AG) into the skip connections, as illustrated in Fig. 4(c). Each attention gate takes the feature maps from the encoder and a gating signal from the decoder as inputs. After adjusting the number of channels, the two are concatenated and then processed through a 1×1 convolution followed by a Sigmoid activation function, thereby generating a weight coefficient map. The feature maps from the decoder provide a reference for analyzing what kind of information the current decoder stage requires more urgently, and enable the skip connections to perform selective filtering on encoder features, automatically suppressing noise and irrelevant information rather than transmitting all signals equally. This mechanism draws on visual-attention theory and enhances the model's awareness of complex structures through dynamic feature weighting, guaranteeing the reliability of imaging in complex geological structures.

In addition, two Dropout layers have been incorporated into the network, whose function is to randomly set neurons to zero according to a specified dropout rate. The advantage of doing so lies in reducing the emergence of similar neurons and avoiding overfitting, thereby enhancing the generalization ability of the network. In this study, two dropout layers are strategically placed at the bottleneck and decoder branches, the dropout rate is set to 0.5. These modifications are expected to improve both the efficiency of network training and the overall performance of imaging optimization.

2.3. Generation of training datasets

Based on the Marmousi and Sigsbee2B models, as shown in Fig. 5(a) and (b), we synthesized seismic data using the acoustic finite-difference forward modeling method. The Marmousi model has a horizontal distance of 17.5 km and a vertical depth of 6.25 km, while the Sigsbee model has a horizontal distance of 20 km and a vertical depth of 6 km. The towed-streamer is positioned on the right side of the source and moves with the source, the cable length is 3000 m. The OBN receivers are deployed on the seabed, with a spacing of 250 m.

The Ricker wavelet is chosen as the source wavelet. To generate data with different frequency characteristics, the dominant frequencies for the towed-streamer and OBN data in the Marmousi model are set to 20 Hz and 15 Hz, respectively, while in the Sigsbee model, they are reduced by 5 Hz each.

In these two velocity models, there exist drastic stratigraphic fluctuations and widespread fault development. We focus on the complex deep structural area, specifically where the migration results from the towed-streamer data are poor but those from OBN data are good. Initially, we obtain imaging results for both towed-streamer and OBN data using the reverse time migration method. Then, normalization is applied to the entire image to ensure training stability.

Due to the limited number of total training samples, we extract a series of patches from the original images using a sliding window (as shown in Fig. 5(c)) to serve as training data, where the patches from the towed-streamer data are used as inputs and those from the OBN data as labels. Generally speaking, larger patch sizes facilitate the network's ability to learn overall structural features but also increase memory consumption during training, whereas smaller patches help conserve memory while focusing more on local details. After considering hardware constraints, training costs, and performance trade-offs, we set the patch size to 128×128 pixels. During this process, we can flexibly adjust the position of data extraction to avoid the interference from shallow acquisition footprints in the OBN images and prevent the introduction of additional noise in the predicted images. Subsequently, we augment the sample size by a factor of 8 through flipping, rotating at various angles, and adding Gaussian white noise of different intensities, in order to enhance the network's learning capability and generalization performance. We randomly select 25% of the dataset as the validation set, with the remainder serving as the training set.

This carefully designed dataset provides a robust foundation for training the deep learning model described in the next section, enabling it to learn the complex mapping from low-quality to high-fidelity migration images.

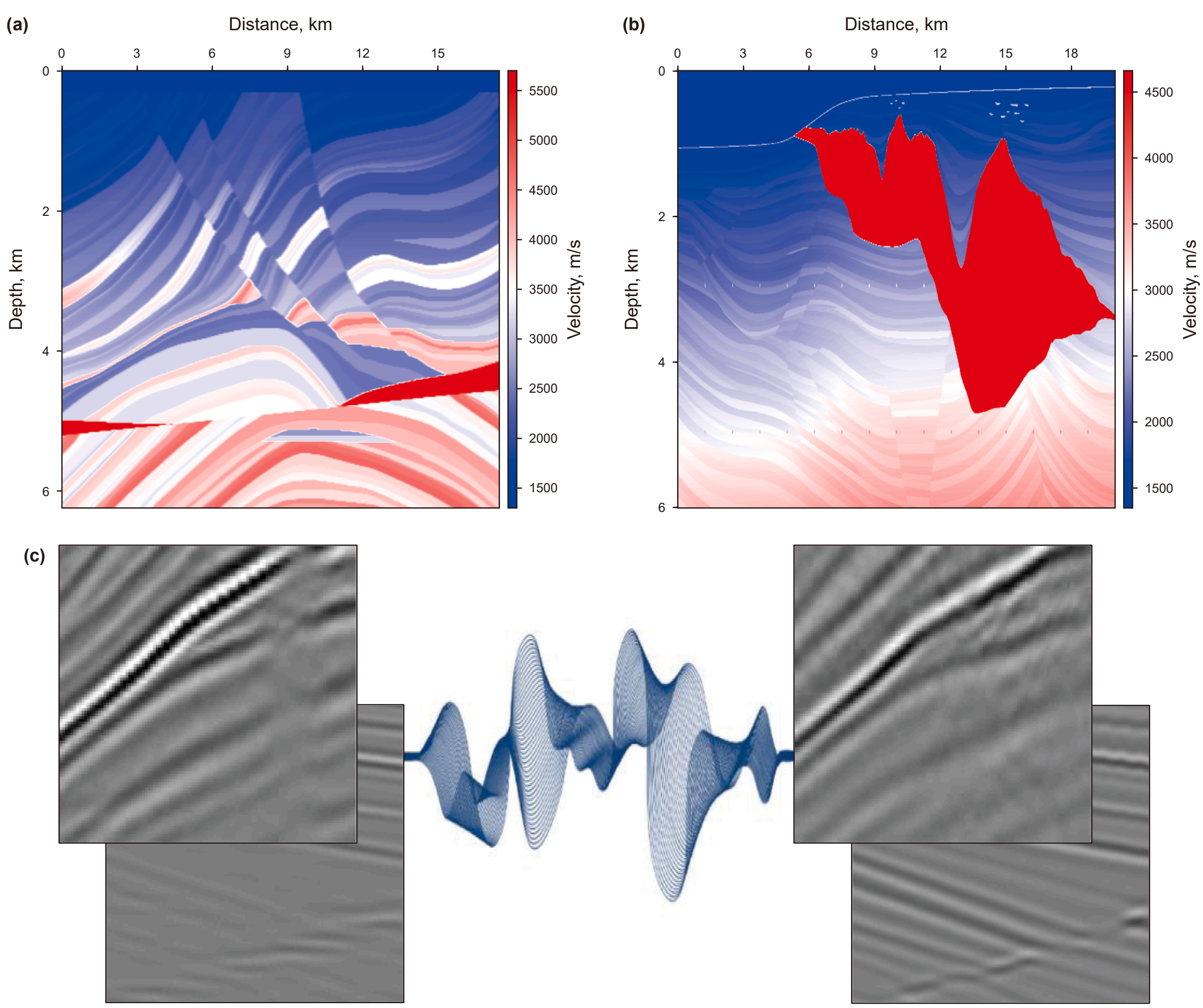

Fig. 5. Generation of datasets. (**a**) Marmousi model, (**b**) Sigsbee2B model, (**c**) examples of training dataset.

2.4. Network training and imaging enhancement

Conventional joint imaging methods typically generate the final image profile by simultaneously imaging towed-streamer and OBN data, which is essentially a linear superposition of the two individual images. This approach, however, is inherently limited: it cannot deliver effective local enhancement in poorly illuminated zones resulting from complex geology, nor can it compensate for acquisition-related discrepancies between the two surveys.

To overcome these limitations, we introduce the concept of imaging matching, which aims to eliminate acquisition discrepancies such as source wavelet differences and further enhance local imaging in poorly illuminated areas. Therefore, we propose an image fusion approach based on imaging matching, which can be described as follows:

$$\widehat{I}(x,z) = \Psi(x,z) \otimes I^{p}_{\mathrm{ts}}(x,z), \tag{13}$$

where $\widehat{I}$ represents the predicted image, Ψ is a filtering operator designed to match the imaging characteristics of towed-streamer data toward those of OBN data.

Based on the constructed training dataset, we implement the proposed U-Net architecture to learn a nonlinear mapping between the towed-streamer and OBN images. This flowchart is illustrated by Fig. 6. The training process can be regarded as a procedure for obtaining the matched filtering operator Ψ in Eq. (13), which characterizes the nonlinear mapping between the input and output data. In contrast, conventional approaches typically solve for the filtering operator through a least-squares problem, in which the relationship between the input and target output is usually assumed to be linear. The primary goal of network training is to build a model that adaptively enhances under-illuminated and structurally complex regions in towed-streamer images by leveraging the superior illumination characteristics of OBN imaging.

Unlike traditional linear stacking approaches that apply uniform weighting across the whole imaging domain, this method employs a data-driven strategy that enables spatially adaptive enhancement. Through supervised learning, the model learns to emphasize structural features in geologically challenging zones—such as deep or shadowed areas—based on the high-fidelity reference images provided by OBN imaging results.

During training, the network is optimized to produce an output that closely approximates the target OBN imaging result. The mapping function is defined as

$$\widehat{I} = Net\left(I^{p}_{\mathrm{ts}}, \theta\right), \tag{14}$$

where *Net* refers to the network architecture, and θ represents the internal parameters of the network. In this case, the role of operator Ψ in Eq. (13) is replaced by the network model. The mean squared error (MSE) loss function is employed here to measure the error between the predicted values and the true values. Subsequently, through the training of the network, the error is gradually minimized. The MSE loss function is described by the following equation:

$$L_{\mathrm{MSE}} = \frac{1}{2}\left\|\widehat{I} - I^{\mathrm{m_1}}_{\mathrm{obn}}\right\|_2^2, \tag{15}$$

where $\|\cdot\|_2^2$ denotes the norm. We use the Adam optimization algorithm to solve the objective function. After training, the model is deployed to enhance full RTM images generated from towed-streamer data.

After completing the network training, the towed-streamer imaging data are processed progressively using the same 128×128 patch size. These patches are extracted with a sliding stride of 40, resulting in approximately two-thirds overlap between adjacent patches. For patches located at the edges of the image, zero-padding is applied to regions outside the imaging area. Meanwhile, to avoid edge artifacts during patch recombination, a Gaussian window function is applied to each patch to taper amplitudes near the boundaries.

The proposed network training framework effectively learns the nonlinear mapping between towed-streamer and OBN images. Leveraging deep learning, it enables localized enhancement of towed-streamer images in complex structural areas, producing outputs with improved illumination and more continuous structural features, the method provides a flexible and scalable solution for deep layer imaging challenges. Meanwhile, this method also leverages the advantages of towed-streamer data to preserve high-quality images of shallow layers while avoiding the acquisition footprint artifacts commonly present in OBN imaging results.

3. Numerical examples

3.1. Training on Sigsbee2B model

To validate the effectiveness of the proposed deep learning-based imaging enhancement strategy, we conduct numerical experiments based on Sigsbee2B model introduced earlier. These experiments are designed to simulate realistic seismic acquisition scenarios and assess the network's ability to enhance towed-streamer imaging results using information derived from OBN data.

Fig. 7 displays the imaging results of simulated towed-streamer and OBN data of the Sigsbee model. Both datasets are obtained through finite-difference forward modeling (as shown in Fig. 7(b) and (c)). The extended SRME algorithm for OBN data, is utilized to separate the down-going first-order multiples from the OBN data. Then, conventional primary RTM is used to image the towed-

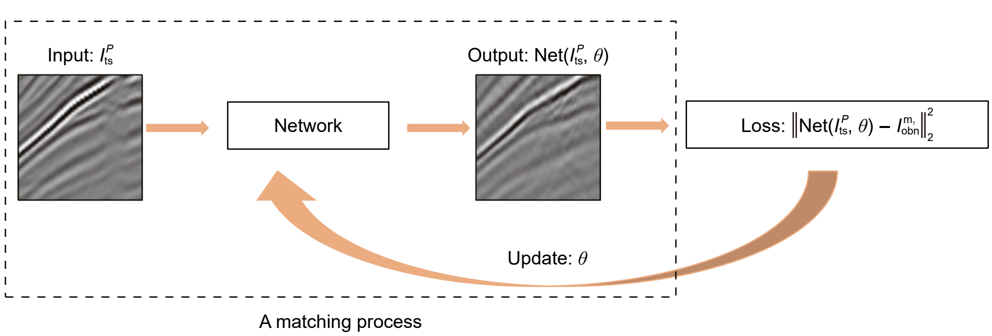

Fig. 6. Flowchart of imaging enhancement based on deep learning.

streamer data, while the mirror migration technique is employed to image the first-order multiples in the OBN data.

In the imaging result of the towed-streamer data (Fig. 7(d)), the limited receiver offset is unfavorable for capturing reflections from steeply dipping formations, leading to insufficient illumination in the arrow-indicated salt-boundary and subsalt areas. In contrast, the OBN observation system offers flexible deployment and enables large-offset acquisition, making it more suitable for probing deep and complex structures. The corresponding image (Fig. 7(f)) clearly and accurately delineates the subsalt structures, showing significantly better illumination than the towed-streamer image in the areas indicated by the arrows. Furthermore, in the imaging result obtained using conventional primary migration method (Fig. 7(e)), issues such as poor shallow illumination and low signal-to-noise ratio caused by sparse deployment of OBNs have been partially resolved in the mirror migration result (Fig. 7(f)), validating the effectiveness of the down-going wave imaging method. These results demonstrate that while towed-streamer data alone struggle to provide sufficient illumination in complex areas, OBN data can offer richer structural information. This also highlights the necessity of integrating these two imaging approaches.

To train the network model, a data-blocking strategy is first applied to generate the training datasets. The images from the towed-streamer data are used as inputs, while those from the OBN data serve as labels. All migrated results required for training are pre-normalized. Then, we extract a total of 396 datasets (128×128) from the yellow region indicated in Fig. 7(a) and apply data augmentation to expand the sample size. It should be noted that only a portion of the deep, poorly illuminated zone indicated in Fig. 7(d) is included in the training. Subsequently, the trained network model performs a single prediction pass over the entire towed-streamer imaging result. This training strategy is designed to evaluate the generalization capability of the network model while avoiding potential adverse effects of normalization on the energy distribution within the enhanced imaging result. The network model is trained for 200 epochs, with a batch size of 4 and learning rate of 1e−3. The training process required 55 min with a memory usage of 11 GB. The convergence behavior is shown in Fig. 8.

First, we evaluated the performance of the network model using localized patches. These patches were selected from the

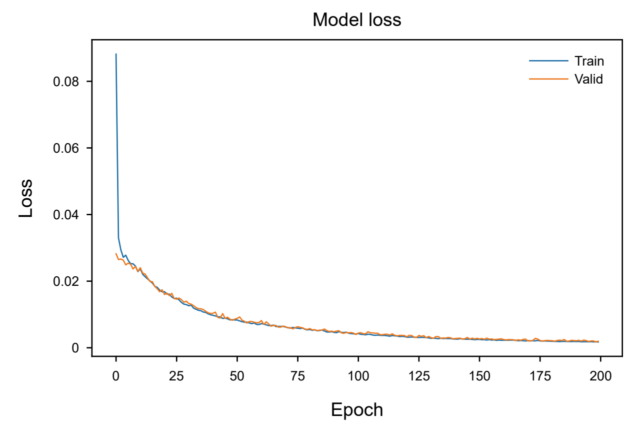

Fig. 8. Loss function curve for training of Sigsbee2B model.

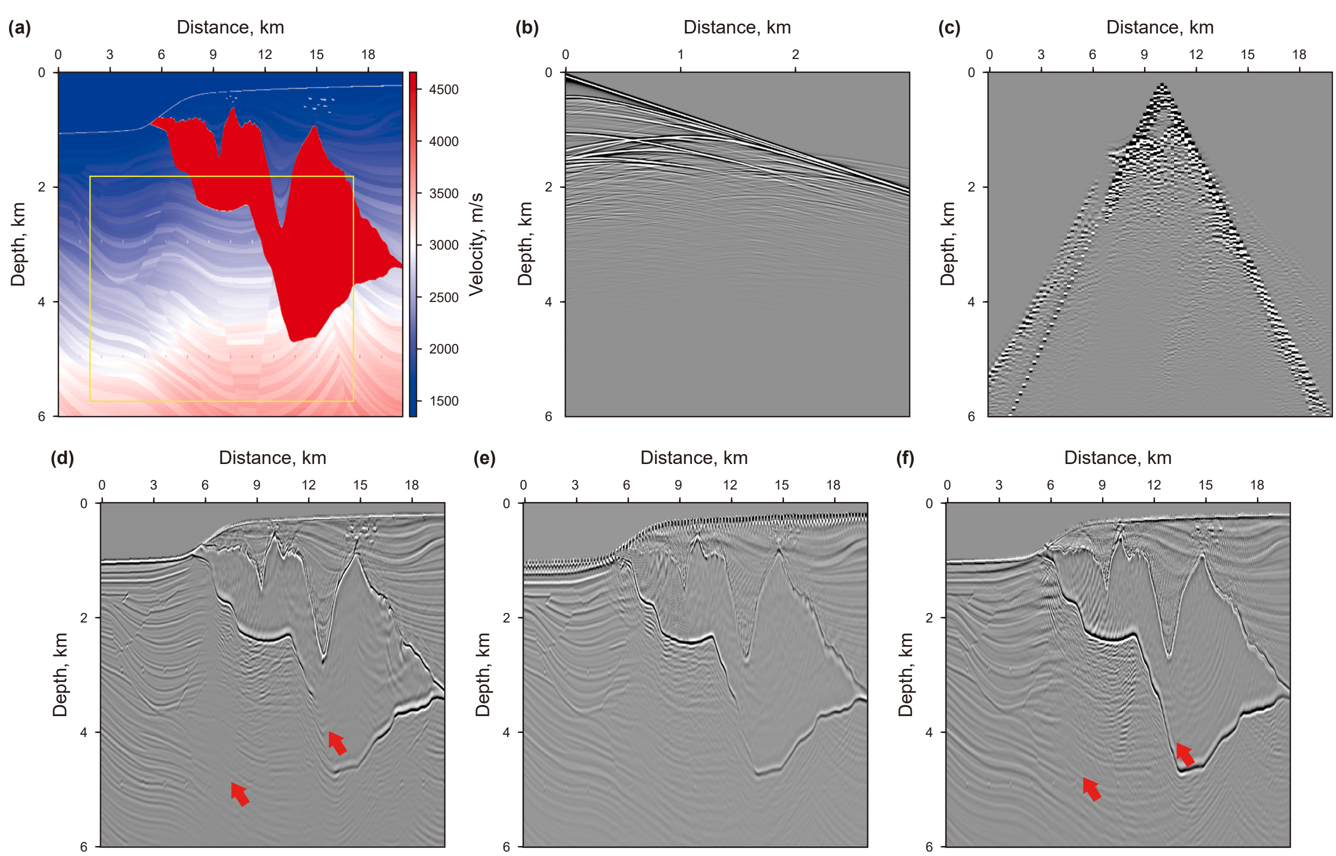

Fig. 7. Imaging results of partial Sigsbee2B model. **(a)** Velocity model, **(b)** towed-streamer data, **(c)** OBN data, **(d)** image of towed-streamer data, **(e)** conventional image of OBN data, **(f)** mirror image of OBN data.

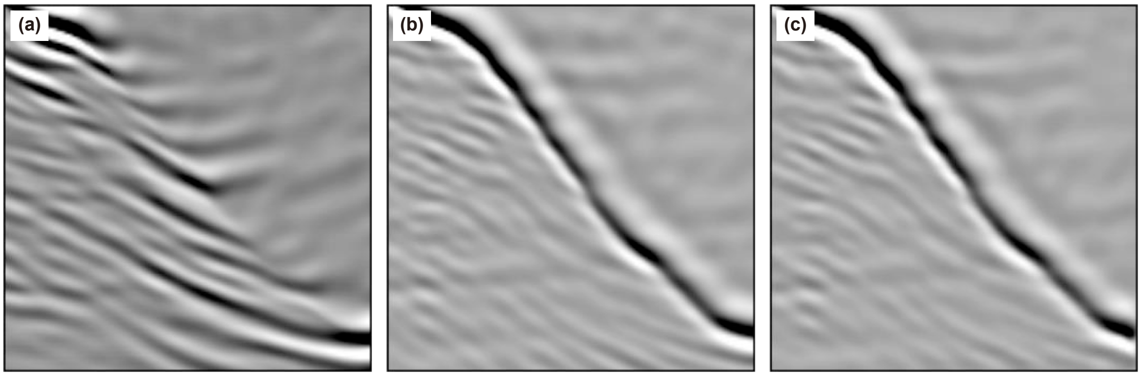

Fig. 9. Localized data analysis of Sigsbee2B model. **(a)** Image of towed-streamer data, **(b)** mirror image of OBN data, **(c)** network enhanced image.

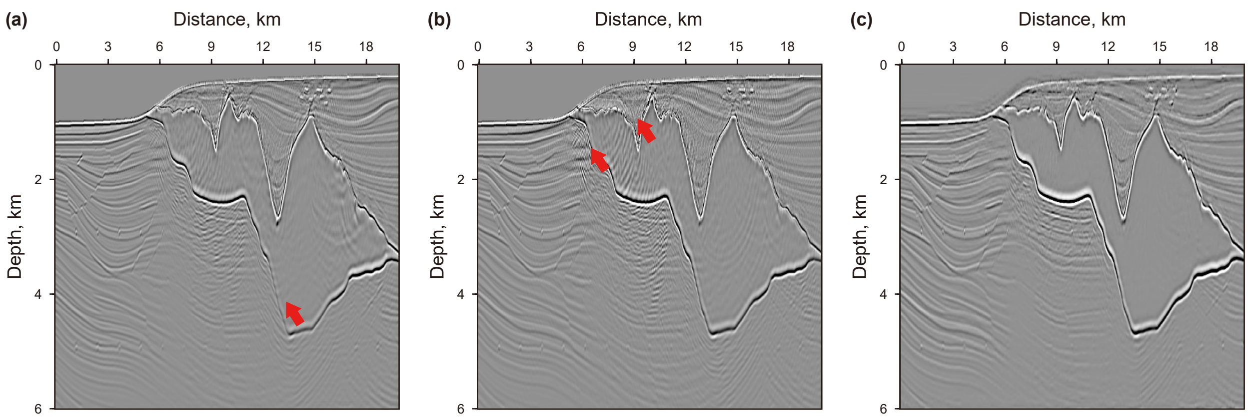

Fig. 10. Joint imaging results of Sigsbee2B model. **(a)** Linear stacking image with a weighted factor of 0.2, **(b)** linear stacking image with a weighted factor of 0.4, **(c)** enhanced image by the deep learning-based method.

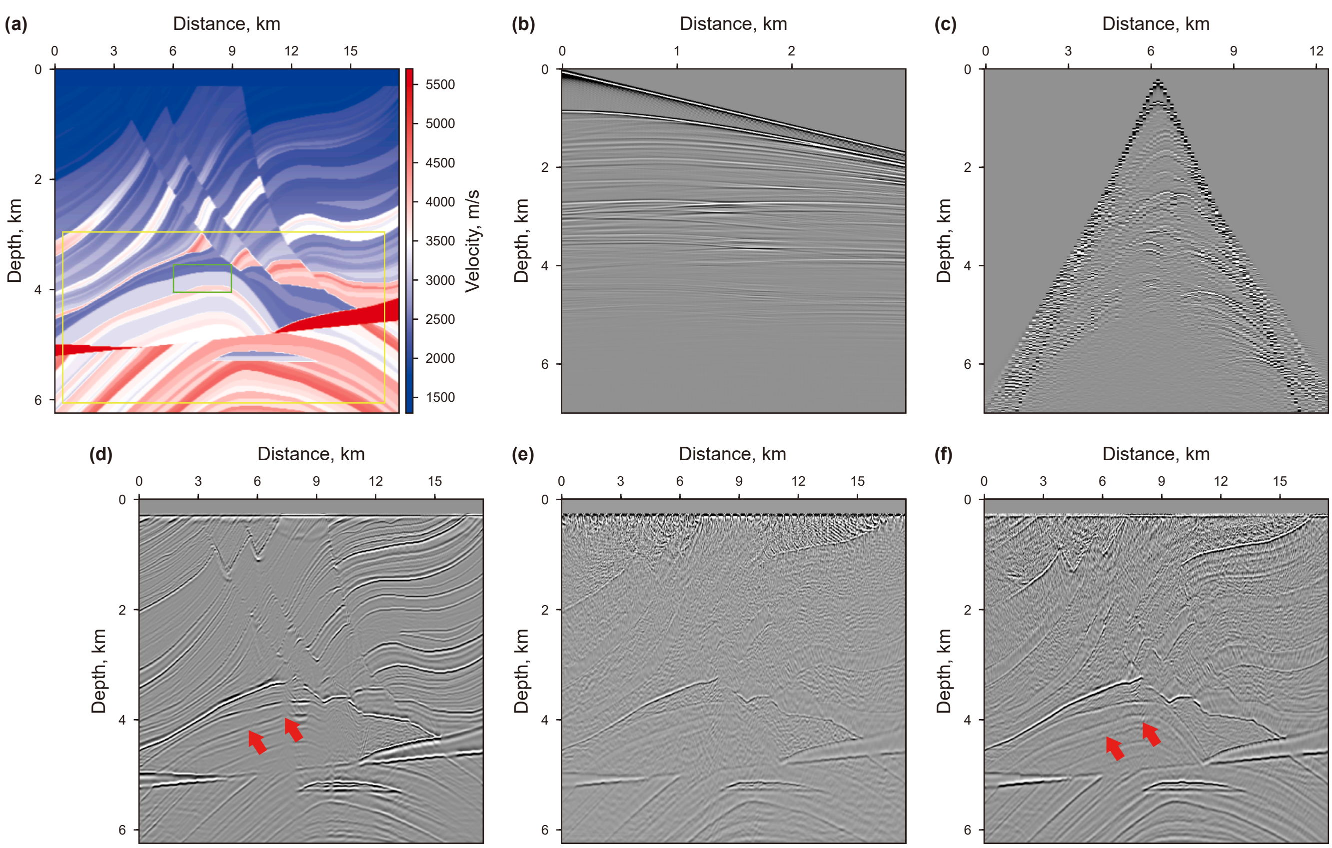

Fig. 11. Imaging results of Marmousi model. **(a)** Velocity model, **(b)** towed-streamer data, **(c)** OBN data, **(d)** image of towed-streamer data, **(e)** conventional image of OBN data, **(f)** mirror image of OBN data.

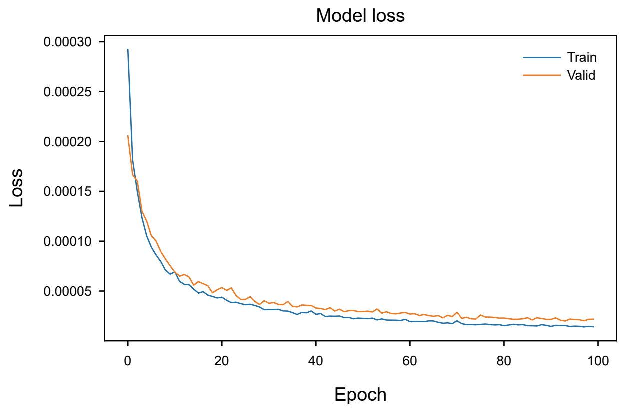

Fig. 12. Loss function curve for training of Marmousi model.

vicinity of the subsalt boundary. As shown in Fig. 9(a), the imaging result of the towed-streamer data in this region is suboptimal, with a poorly defined salt boundary. In contrast, the network-predicted result (Fig. 9(c)) exhibits clear and continuous events, achieving an imaging quality comparable to that of the OBN data (Fig. 9(b)). The results verify the effectiveness and robustness of the proposed method. Subsequently, all patches are processed using the trained network and recombined to generate the final enhanced image.

Then, we generated optimized imaging results based on both the conventional linear weighted stacking strategy and the proposed network-based method, as shown in Fig. 10. Fig. 10(a) and (b) present the weighted stacking results obtained by combining the streamer image with the OBN image using weighting factors of 0.2 and 0.4, respectively. Fig. 10(c) displays the imaging result enhanced by the proposed network-based approach. The linear weighted stacking method exhibits clear limitations: it either fails to enhance the poorly illuminated zones (arrows in Fig. 9(a)) or introduces migration noise (arrows in Fig. 10(b)). In contrast, the deep learning-based approach achieves a superior result (Fig. 10(c)), preserving the imaging advantages of the streamer data in shallow layers while avoiding the excessive introduction of acquisition footprint noise from the OBN data. This is attributed to the flexible extraction of training data and the highly nonlinear capability of the network model, which circumvent the limitations of conventional linear weighting methods. Moreover, the prediction time required is only 2 s, demonstrating that a well-trained network model can rapidly and effectively complete imaging optimization tasks.

3.2. Transfer learning for Marmousi model

Since samples generated from a single model cannot adequately represent the influences of different acquisition parameters and geological structures, the network may fail to effectively learn the required features. Therefore, we incorporate additional datasets into the original network model for further training.

To further enhance network performance, we generated a new training dataset using the Marmousi model with imaging results shown in Fig. 11. The towed-streamer imaging result (Fig. 11(d)) not only reveals poor imaging of the steeply dipping interfaces in the central region but also displays discontinuous seismic events in the arrow-highlighted areas, primarily due to insufficient illumination of deeper zones by the towed-streamer system. In contrast, the conventional OBN imaging and the mirror imaging results (Fig. 11(e) and (f)) demonstrate the advantages of downgoing wave imaging. Fig. 11(f) exhibits superior signal-to-noise ratio with clearly delineated deep structures, making it suitable for network training.

To enhance the model's generalization capability and improve training efficiency, transfer learning is adopted to implement the training on the Marmousi model. The previously obtained training results on the Sigsbee model were treated as “pre-trained” parameters and loaded into the network, replacing conventional initialization methods. The resulting network can be considered an adjustment of the existing model rather than training from scratch. This approach enables faster convergence during training and reduces the demand for new dataset size to some extent, effectively saving computation costs.

In this step of network training, the learning rate is set to 1e−4. We freeze the residual blocks in the first three down-sampling

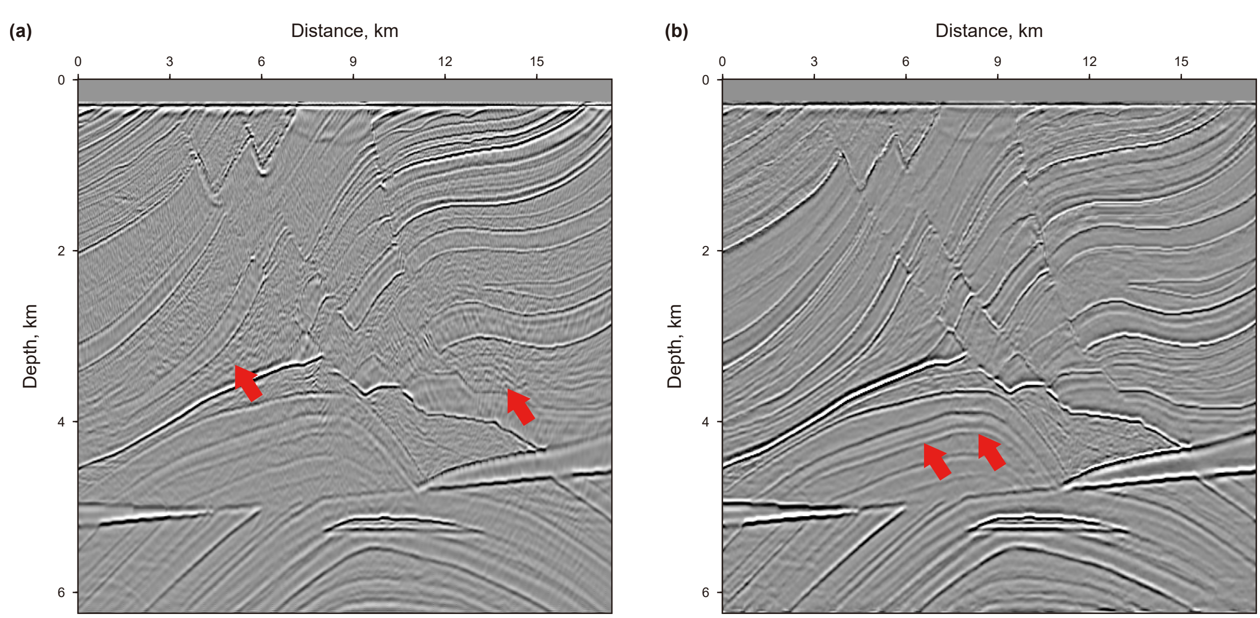

Fig. 13. Joint imaging results of Marmousi model. **(a)** Linear stacking image, **(b)** enhanced image by the deep learning-based method.

stages of the encoder, excluding them from training. A total of 120 datasets are generated, and data augmentation is applied. The network is trained for 100 epochs with a batch size of 4. The training process required a total of 8 min, and the loss curve is illustrated in Fig. 12.

The final joint imaging result is presented in Fig. 13. Due to the broader influence of acquisition footprints, where migration noise (arrows in Fig. 13(a)) aliases with certain target imaging zones, the weighted stacking image fails to achieve satisfactory imaging enhancement. In contrast, the network-predicted image demonstrates relatively better performance owing to strategic cropping of training data. As indicated by the arrows in Fig. 13(b), the discontinuous events observed in the original towed-streamer image have been effectively recovered, while migration noise in the shallow layers remains minimal, allowing for clear delineation of reflection interfaces.

To conduct a detailed analysis of the imaging results, we focus on the regions within the green box in Marmousi model (shown in Fig. 11(a)) and generate waveforms from the corresponding migrated sections, as illustrated in Fig. 14. By comparing the migration results and the reflectivity model (Fig. 14(a)), it is visually evident from the waveforms that the Marmousi model displays discontinuities in the events. Comparatively, OBN image provide a more accurate representation of this area. After optimizing the towed-streamer image using a neural network, as demonstrated in Fig. 14(d), the morphology and energy of the events are significantly improved, enabling a more precise reflection of the interface characteristics.

3.3. Field data test

Finally, we employ a field dataset to evaluate the performance of the proposed method (see Fig. 15). The survey area spans 17.5 km horizontally and extends to a depth of 5.7 km. For the towed-streamer data, the shot interval is 50 m, with acquisition proceeding from left to right across the survey area. Receivers are

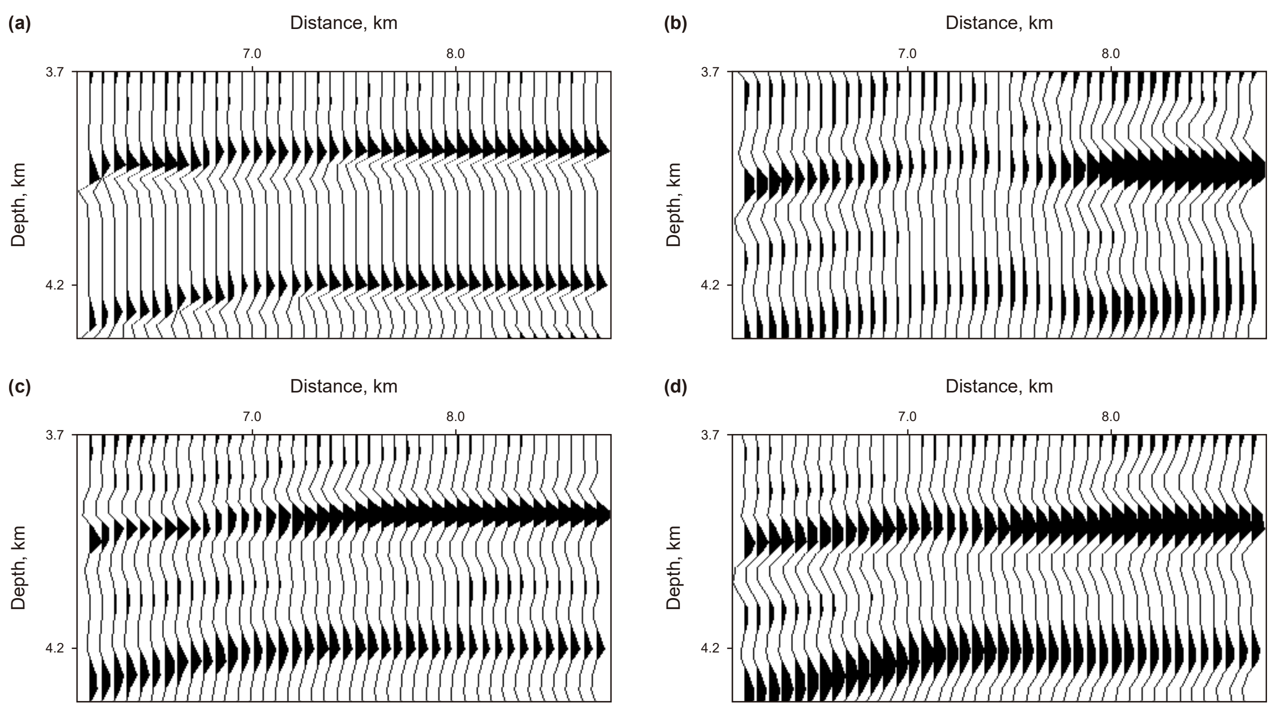

Fig. 14. Waveform analysis of Marmousi model. (**a**) Reflectivity model, (**b**) towed-streamer image, (**c**) OBN image, (**d**) network enhanced image.

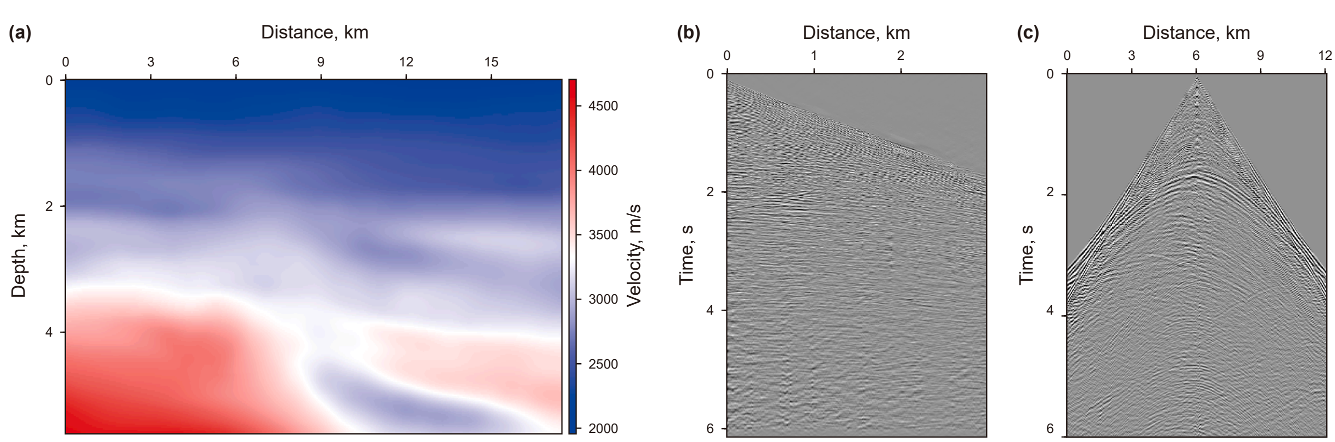

Fig. 15. Field data. (**a**) Migration velocity model, (**b**) towed-streamer data, (**c**) OBN data.

positioned to the left of the shot points, with a trace spacing of 12.5 m. The minimum offset is 170 m, and the maximum offset is 3000 m. For the OBN data, the shot interval is 37.5 m, the receiver spacing is 250 m, the water depth ranges from 25 to 30 m. The minimum offset is 70 m, and the maximum offset is 6100 m. The proposed approach focuses on enhancing areas of poor illumination and addressing imaging blind zones in the original streamer data, which is crucial in complex subsurface environments. By leveraging deep learning, we can effectively capture the intricate relationship between the imaging characteristics of towed-streamer data and OBN data.

The imaging results of the towed-streamer and OBN data are shown in Fig. 16(a) and (b), respectively. Due to differences in characteristics such as frequency bandwidth between the two datasets, distinct event features are observed in their respective migration results. Arrows in Fig. 16(a) indicate regions with poor towed-streamer imaging quality, which will serve as the target for imaging enhancement.

Regarding the waveform matching between towed-streamer and OBN data, although certain general patterns exist in actual acquisition (such as richer low-frequency information in OBN data), our samples remain insufficient. To ensure effective matching, we continue to employ a transfer learning strategy here. A total of 90 datasets (128×128) were acquired from regions with low noise impact and relatively accurate OBN images. Meanwhile, the target area for imaging enhancement did not directly participate in training and will serve as a test for the supplementary illumination performance of the network model during final application. In this transfer learning setup, the encoder parameters are frozen, and only the decoder section is trained, with the learning rate set to 1e−4. The network is trained for 125 epochs with a batch size of 4, and required a total of 7 min.

The entire towed-streamer image is then used as input for prediction to generate the enhanced imaging result. As shown in Fig. 16(d), the prediction process is completed in 4 s. As can be observed from the figure, the waveform of the towed-streamer image is successfully matched after network processing. The weakly-illuminated zone which is not involved in training is effectively compensated. Noise in the shallow layers of OBN image is also suppressed to a certain extent. This further verifies the feasibility and effectiveness of the proposed method.

During the network prediction process, features such as waveform and energy from the input towed-streamer images are matched to their corresponding OBN images. Compared with conventional weighted stacking method, the process is also computationally efficient and can be performed very rapidly. Consequently, we next focus on a discussion of the resulting image quality. The signal-to-noise ratios of the images obtained by the

Table 1
SNR analysis of joint images.

Method	Sigsbee2B	Marmousi	Field data
Linear stacking	13.21 dB	13.66 dB	7.92 dB
Deep learning	15.76 dB	16.97 dB	9.30 dB

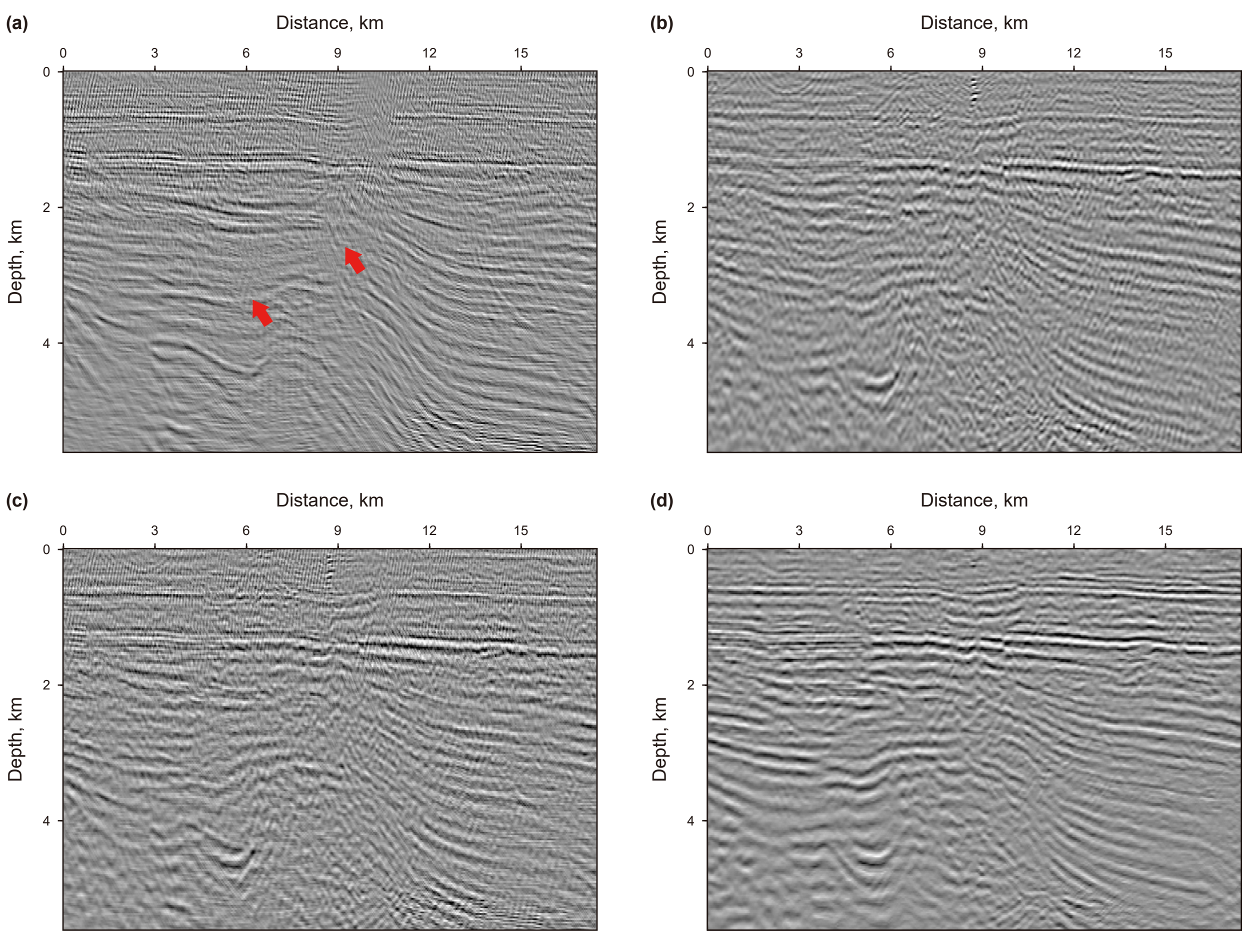

Fig. 16. Imaging results of field data. **(a)** Image of towed-streamer data, **(b)** mirror image of OBN data, **(c)** linear stacking image, **(d)** network enhanced image.

proposed deep learning method and the conventional weighted stacking method are summarized in Table 1. The network-predicted image exhibits a higher signal-to-noise ratio compared to the stacked image, demonstrating the effectiveness of the proposed approach in suppressing migration noise. These results further confirm significant advantage of the proposed method over the conventional linear weighted stacking method in terms of final imaging quality.

4. Conclusions

In this study, we propose a deep learning-based method to enhance towed-streamer imaging by integrating information from OBN data. To address the limitations of towed-streamer imaging in complex and deep geological settings, a neural network is trained to learn the nonlinear mapping between deep-layer imaging results from towed-streamer and OBN data. This enables the network to supplement and enhance towed-streamer images using the superior deep illumination provided by OBN acquisitions. The feasibility and effectiveness of this approach are verified through numerical experiments on two complex velocity models, demonstrating that the trained neural network can effectively enhance quality of deep-layer imaging for towed-streamer data. Moreover, the method achieves accurate feature matching, avoids shallow-layer noise in sparse OBN imaging, and produces higher-quality imaging results.

CRediT authorship contribution statement

Zhi-Na Li: Writing – review & editing, Supervision, Conceptualization. **He-Xiang Zhang:** Writing – original draft, Validation, Methodology, Data curation. **Zhen-Chun Li:** Supervision, Conceptualization. **Zi-Lin He:** Formal analysis, Data curation. **Qi Zhang:** Formal analysis, Data curation. **Bo-Xiong Zhao:** Validation, Formal analysis. **Zhi-Chuan Yu:** Validation, Formal analysis. **Qiang Xu:** Supervision, Resources. **Ming-Qiang Zhang:** Data curation.

Declaration of competing interests

The authors declare that they have no known competing financial interests or personal relationships that could have appeared to influence the work reported in this paper.

Acknowledgments

Thanks to the support from the National Natural Science Foundation of China (42574164), Fund of State Key Laboratory of Deep Oil and Gas, China University of Petroleum (East China) (SKLDOG2024-ZYTS-05), Qingdao Natural Science Foundation (24-4-4-zrjj-186-jch).

References

Aharchaou, M., Baumstein, A., 2020. Deep learning-based artificial bandwidth extension: Training on ultrasparse OBN to enhance towed-streamer FWI. Lead. Edge 39 (10), 718–726. https://doi.org/10.1190/tle39100718.1.

Alerini, M., Traub, B., Ravaut, C., et al., 2009. Prestack depth imaging of ocean-bottom node data. Geophysics 74 (6), WCA57–WCA63. https://doi.org/10.1190/1.3204767.

Alfarhan, M., Ravasi, M., Alkhalifah, T., 2023. A deep learning-based inverse hessian for full-waveform inversion. In: Third International Meeting for Applied Geoscience & Energy Expanded Abstracts, pp. 635–639. https://doi.org/10.1190/image2023-3908592.1.

Barr, F.J., 1997. Dual-sensor OBC technology. Lead. Edge 16 (1), 45–52. https://doi.org/10.1190/1.1437427.

Cheng, S.-J., Shi, X.-C., Mao, W.-J., et al., 2023. Elastic seismic imaging enhancement of sparse 4C ocean-bottom node data using deep learning. IEEE Trans. Geosci. Rem. Sens. 61, 1–14. https://doi.org/10.1109/TGRS.2023.3275614.

Granger, P., Manin, M., Boelle, J., et al., 2005. Autonomous 4C nodes used in infill areas to complement streamer data, deepwater case study. In: SEG Technical Program Expanded Abstracts, pp. 84–87. https://doi.org/10.1190/1.2144444, 2005.

Halpert, D., 2018. Deep learning-enabled seismic image enhancement. In: SEG Technical Program Expanded Abstracts, pp. 2081–2085. https://doi.org/10.1190/segam2018-2996943.1, 2018.

Ikelle, L.T., 1999. Combining two seismic experiments to attenuate free-surface multiples in OBC data. Geophys. Prospect. 47 (2), 179–193. https://doi.org/10.1046/j.1365-2478.1999.00125.x.

Li, H.-Y., Gu, R.-Y., Hutson, J., et al., 2022. Subsalt image optimization in the Gulf of Mexico combining sparse OBN and legacy streamer data. In: Second International Meeting for Applied Geoscience & Energy, pp. 2942–2946. https://doi.org/10.1190/image2022-3750803.1.

Li, Z.-N., Li, Z.-C., Wang, P., et al., 2017. Reverse time migration of multiples based on different-order multiple separation. Geophysics 82 (1), S19–S29. https://doi.org/10.1190/geo2015-0710.1.

Liu, Z.-L., Chen, Y.-Q., Schuster, G., 2020. Deep convolutional neural network and sparse least-squares migration. Geophysics 85 (4), WA241–WA253. https://doi.org/10.1190/geo2019-0412.1.

Malikov, R., Yusubova, T., Shahsenov, I., 2024. Deep learning approach for denoising and resolution enhancement of poststack seismic data. In: Fourth International Meeting for Applied Geoscience & Energy, pp. 2048–2052. https://doi.org/10.1190/image2024-4090529.1.

Pacal, E., Stewart, R., Baysal, E., et al., 2015. Seismic imaging with ocean-bottom nodes (OBN): Mirror migration technique. In: SEG Technical Program Expanded Abstracts, pp. 4039–4043. https://doi.org/10.1190/segam2015-5886915.1, 2015.

Poole, G., 2021. Least-squares multiple imaging constrained jointly by OBN and towed-streamer data. In: 82nd EAGE Annual Conference & Exhibition, pp. 1–5. https://doi.org/10.3997/2214-4609.202113070.

Shi, P.-F., Xu, X.-W., Fan, X.-N., et al., 2024. LL-UNet++: UNet++ based nested skip connections network for low-light image enhancement. IEEE Trans. Comput. Imaging 10, 510–521. https://doi.org/10.1109/TCI.2024.3378091.

Singh, S., Tsvankin, I., Naeini, E.Z., 2021. Elastic FWI for orthorhombic media with lithologic constraints applied via machine learning. Geophysics 86 (4), R589–R602. https://doi.org/10.1190/geo2020-0512.1.

Sun, J.-X., Yang, J.-D., Huang, J.-P., et al., 2023a. LsmGANs: Image-domain least-squares migration using a new framework of generative adversarial networks. IEEE Trans. Geosci. Rem. Sens. 61, 1–13. https://doi.org/10.1109/TGRS.2023.3304726.

Sun, J., Arash, J., Julian, H., 2023b. Deep learning-based Vz-noise attenuation for OBS data. In: Third International Meeting for Applied Geoscience & Energy Expanded Abstracts, pp. 1480–1484. https://doi.org/10.1190/image2023-3910189.1.

Torres, K., Sacchi, M., 2021. Deep learning based least-squares reverse-time migration. In: First International Meeting for Applied Geoscience & Energy Expanded Abstracts, pp. 2709–2713. https://doi.org/10.1190/segam2021-3581036.1.

Walker, C., Zhou, Z.-Z., Lii, X., 2023. Hybrid streamer/sparse OBN imaging offshore Norway. In: Third International Meeting for Applied Geoscience & Energy Expanded Abstracts, pp. 1628–1632. https://doi.org/10.1190/image2023-3915690.1.

Wong, M., Ronen, S., Biondi, B., 2012. Joint imaging with streamer and OBN data. In: SEG Technical Program Expanded Abstracts, pp. 1–5. https://doi.org/10.1190/segam2012-0863.1, 2012.

Wu, B., Yao, G., Ma, X., et al., 2024. Least-squares reverse time migration of simultaneous sources with deep-learning-based denoising. Geophysics 89 (3), S289–S299. https://doi.org/10.1190/geo2023-0320.1.

Yang, H.-C., Zhang, J.-Z., 2022. Image-domain least-square reverse-time migration of combined towed-streamer and OBN data. Chin. J. Geophys. 65 (10), 4099–4110. https://doi.org/10.6038/cjg2022P0359 (in Chinese).

Yu, P.-F., Geng, J.-H., Sun, M.-A., 2021. Joint ERTM of TS and sparse OBN/OBS data. In: First International Meeting for Applied Geoscience & Energy Expanded Abstracts, pp. 2774–2778. https://doi.org/10.1190/segam2021-3581463.1.

Yu, P.-F., Chu, M.-Z., Xu, Y.-X., et al., 2023. Joint elastic reverse time migration of towed streamer and sparse ocean-bottom seismic node hybrid data. Geophysics 88 (1), S47–S57. https://doi.org/10.1190/geo2021-0333.1.

Zhang, D., Leeuw, M., Verschuur, E., 2021. Deep learning-based seismic surface-related multiple adaptive subtraction with synthetic primary labels. In: First International Meeting for Applied Geoscience & Energy Expanded Abstracts, pp. 2844–2848. https://doi.org/10.1190/segam2021-3584041.1.

Zhong, R., Ji, S., Xuan, Y., et al., 2014. Incorporating streamer data for OBN free-surface multiple prediction – A case study in deep-water Gulf of Mexico. In: SEG Technical Program Expanded Abstracts. pp. 4108–4112. https://doi.org/10.1190/segam2014-0322.1.